

1

Supplementary Information

2

Ferroelectric resistance switching in Pt/Fe/BiFeO₃/SrRuO₃/SrTiO₃

3

heterostructures

4

5

Wanchao Zheng¹, Yuchen Wang¹, Chao Jin¹, Ruihua Yin¹, Dong Li², Ping Wang¹,

6

Shasha Liu¹, Xinyue Wang¹, Dongxing Zheng¹, and Haili Bai^{1,*}

7

8

¹*Tianjin Key Laboratory of Low Dimensional Materials Physics and Processing*

9

Technology, School of Science, Tianjin University, Tianjin 300350, People's Republic

10

of China

11

²*Tianjin International Center for Nanoparticles and Nanosystems, Tianjin University,*

12

Tianjin 300072, People's Republic of China

13

14

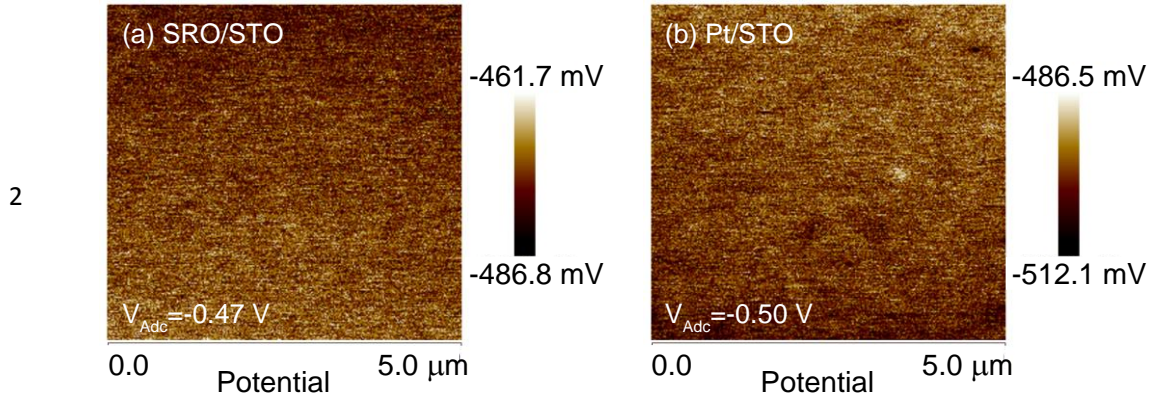
15

16

* Author to whom all correspondence should be addressed.

E-mail: baihaili@tju.edu.cn

1 S1. KPFM patterns

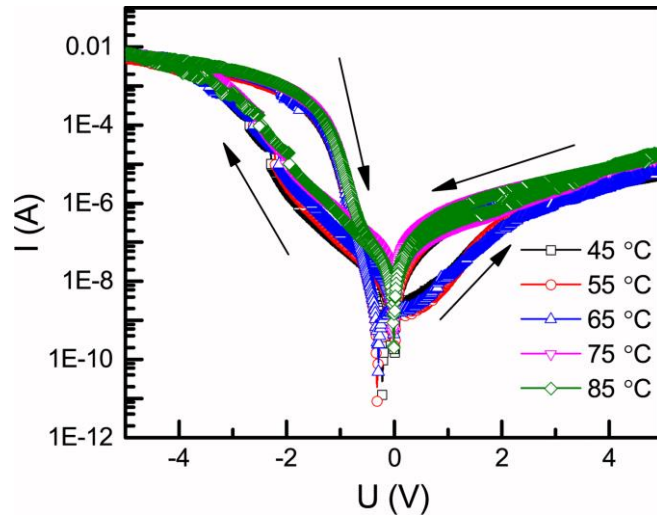


3 **Fig. S1** KPFM patterns of (a) the SRO/STO and (b) the Pt/STO heterostructures in a
4 $5 \times 5 \mu\text{m}^2$ area.

5 Fig. S1 shows the KPFM patterns of the SRO/STO and the Pt/STO
6 heterostructures. The calculated work function φ can be written as $\varphi = \varphi_{\text{tip}} - eV_{\text{Adc}}$,
7 where φ_{tip} (4.81 eV) is the work function of the tip and V_{Adc} is the average surface
8 potential of the sample. In Fig. S1, the V_{Adc} of the SRO and the Pt layers are -0.47 and
9 -0.50 V, respectively. Thus, the calculated work function of the SRO and the Pt are
10 5.28 and 5.31 eV. The calculated work function of the Pt is consistent with the ideal
11 value (5.3 eV), but the calculated work function of the SRO is more than the ideal
12 value (5.2 eV),¹ which is related to the quality of the SRO layer.

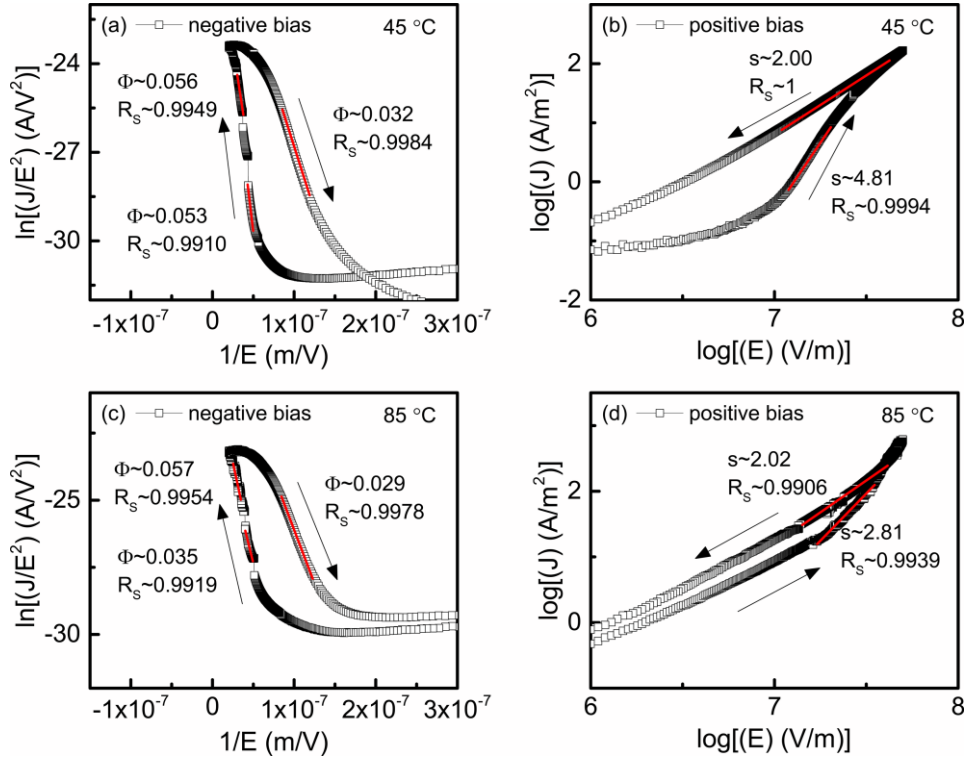
13

1 S2. I - V curves at different temperatures



3 **Fig. S2** I - V curves for the Pt/Fe/BFO/SRO heterostructure at 45, 55, 65, 75 and
4 85 °C.

5 In this work, the temperature is controlled by the thermostatic heater HP-2525.
6 Firstly, the Pt/Fe/BFO/SRO heterostructure is placed on the thermostatic heater
7 HP-2525. Then, we set the temperature by the thermostatic heater HP-2525. When the
8 temperature is stable for 10 minutes, the I - V curves of the Pt/Fe/BFO/SRO
9 heterostructure are measured. Fig. S2 shows the I - V curves of the Pt/Fe/BFO/SRO
10 heterostructure at different temperatures. The obvious bipolar RS behaviors are
11 observed, demonstrating that the electrical property of the Pt/Fe/BFO/SRO
12 heterostructure around room temperature is stable. When the temperature is higher
13 than 75 °C, an obvious signal vibration is observed in Fig. S2. Since the resistance in
14 the Pt/Fe/BFO/SRO heterostructures is related to the ferroelectric polarization, the
15 signal vibration may be resulted from the influence of the temperature on the
16 ferroelectric polarization. With the increase of the temperature, the polarization



1

2 **Fig. S3** (a) $\ln(J/E^2)-1/E$ and (b) $\log(J)-\log(E)$ plots for the Pt/Fe/BFO/SRO
 3 heterostructures at 45 °C. (c) $\ln(J/E^2)-1/E$ and (d) $\log(J)-\log(E)$ plots for the
 4 Pt/Fe/BFO/SRO heterostructures at 85 °C. The s represents the slope of the curve. The
 5 Φ is the barrier height. The R_s is the R -square value of the fitting result.

6 switching becomes easier.² Moreover, for the same applied voltage, the current at high
 7 temperature is more than the current at low temperature. Thus, with the increase of the
 8 temperature, the injected charges accumulate easily at the electrode/BFO interface,
 9 and induce the pinned ferroelectric domains at the electrode/BFO interface.³ Further,
 10 the pinned ferroelectric domains form the channel, leading to the signal vibration.

11 In order to further investigate the conductivity mechanism, the $I-V$ curves of the
 12 Pt/Fe/BFO/SRO heterostructure at 45 and 85 °C are fitted, as shown in Fig. S3
 13 According to the fitting results, the conductivity mechanisms are the interface-limited

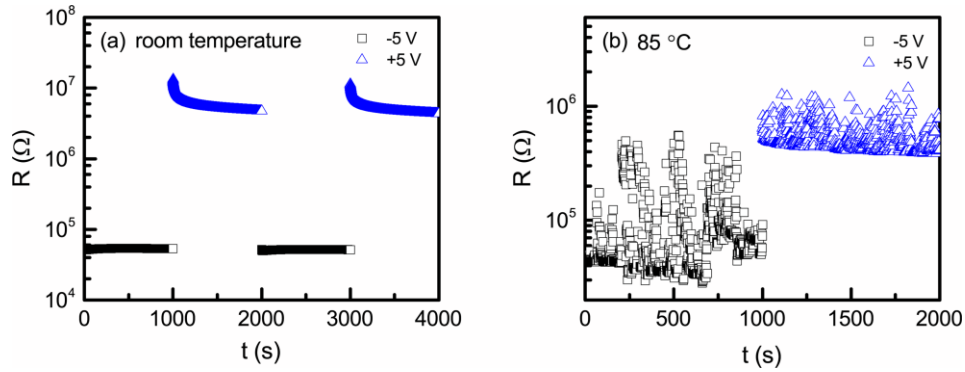
1 FN tunneling mechanism in the negative V and the SCLC mechanism in the positive V .

2 Therefore, the temperature has no influence on the conductivity mechanisms of the

3 Pt/Fe/BFO/SRO heterostructure.

4

1 S3. Retentivity testing



2

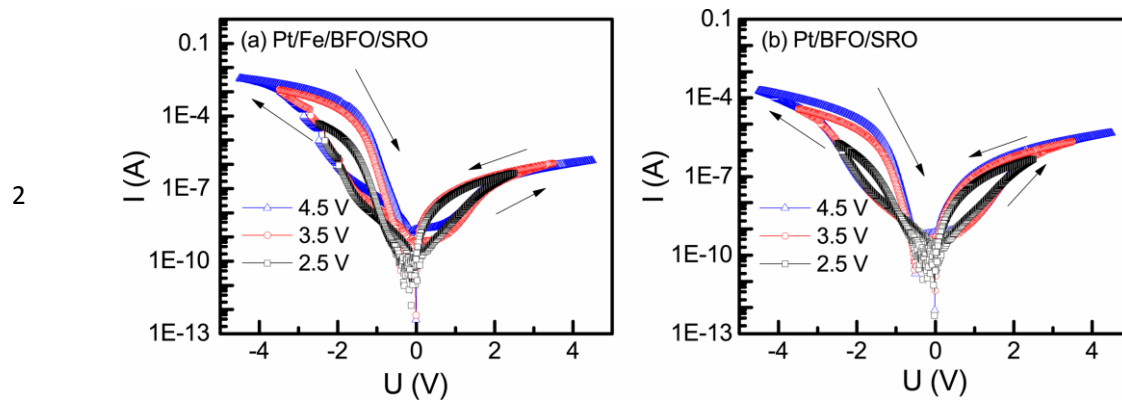
3 **Fig. S4** Retentivity of the HRS and the LRS for the Pt/Fe/BFO/SRO heterostructure
4 after applying +5 and -5 V pulse voltages at (a) room temperature and (b) 85 °C.

5 Fig. S4 shows the retentivity of the HRS and the LRS for the Pt/Fe/BFO/SRO
6 heterostructure at room temperature. Those results demonstrate that the resistance
7 degradation for HRS is intrinsic and may be related to the oxygen vacancies migration.
8 While the Pt/Fe/BFO/SRO heterostructure is poling by the positive pulse voltage, the
9 positive polarization charges and the oxygen vacancies are migrating toward the
10 BFO/SRO interface. When the positive pulse voltage is removed and the read voltage
11 is applied, the oxygen vacancies are gradually far from the BFO/SRO interface due to
12 the electrostatic repulsion interaction of the positive polarization charges and the
13 impact of the read voltage. Since the positive polarization charges and the oxygen
14 vacancies lead to the increase of the depletion layer width, the decrease of the oxygen
15 vacancies around the BFO/SRO interface causes the decrease of the depletion layer
16 width, which induces the resistance degradation for the HRS. Fig. S4(b) shows the
17 retentivity of the HRS and the LRS at 85 °C. The obvious signal vibration is observed,
18 which may be resulted from the influence of the temperature on the ferroelectric

1 polarization. Although the temperature affects the electrical property of the
2 Pt/Fe/BFO/SRO heterostructure, the ratio of the HRS/LRS is ~6.1 is still observed in
3 Fig. S4(b).

4

1 **S4. I - V curves with different applied voltages**



3 **Fig. S5** I - V curves for (a) the Pt/Fe/BFO/SRO and (b) the Pt/BFO/SRO
4 heterostructures. The applied voltage sweeps along $0 \rightarrow -V_{\max} \rightarrow 0 \rightarrow V_{\max} \rightarrow 0$. The V_{\max}
5 is 2.5, 3.5, 4.5 V, and the step is 10 mV. The arrows represent the sweep direction of
6 the applied voltage.

1

- 2 1. D. Li, D. Zheng, C. Jin, W. Zheng and H. Bai, *ACS Appl. Mater. Interfaces*, 2018,
3 **10**, 19836–19843.
- 4 2. J. Wu and J. Wang, *J. Appl. Phys.*, 2010, 108, 094107.
- 5 3. X. Zou, L. You, W. Chen, H. Ding, D. Wu, T. Wu, L. Chen and J. Wang, *ACS*
6 *NANO*, 2012, 6, 8997–9004.